Global sonde datasets do not support a mesoscale transition in the turbulent energy cascade

Thomas D. DeWitt,[a] Timothy J. Garrett,[a]

[a] *University of Utah*

Corresponding author: Timothy J. Garrett, Tim.Garrett@utah.edu

ABSTRACT: Conceptual and theoretical models describing the dynamics of the atmosphere often assume a hierarchy of dynamic regimes, each operating over some limited range of spatial scales. The largest scales are presumed to be governed by quasi-two-dimensional geostrophic turbulence, mesoscale dynamics by gravity waves, and the smallest scales by 3D isotropic turbulence. In theory, this hierarchy should be observable as clear scale breaks in turbulent kinetic energy spectra as one physical mechanism transitions to the next. Here, we show that this view is not supported by global dropsonde and radiosonde datasets of horizontal winds. Instead, the structure function for horizontal wind calculated for vertical separations between 200 m and 8 km has a Hurst exponent of $H_v \approx 0.6$, which is inconsistent with either gravity waves ($H_v = 1$) or 3D turbulence ($H_v = 1/3$). For horizontal separations between 200 km and 1800 km, the Hurst exponent is $H_h \approx 0.4$, which is inconsistent with quasi-geostrophic dynamics ($H_h = 1$). We argue that sonde observations are most consistent with a lesser known "Lovejoy-Schertzer" model for stratified turbulence where, at all scales, the dynamics of the atmosphere obey a single anisotropic turbulent cascade with $H_v = 3/5$ and $H_h = 1/3$. While separation scales smaller than 200 m are not explored here due to measurement limitations, the analysis nonetheless supports a single cohesive theoretical framework for describing atmospheric dynamics, one that might substitute for the more traditional hierarchy of mechanisms that depends on spatial scale.

1. Introduction

The dynamics of Earth's atmosphere are commonly characterized as being governed by three-dimensional Kolmogorov turbulence at the smallest dynamical scales, gravity waves at the mesoscale, and quasi-geostrophic turbulence at the largest scales (Charney 1971; Gage and Nastrom 1986; Lindborg 1999). Combined, this "transition" paradigm partitions these regimes according to their respective wavenumber spectra for kinetic energy, where an isotropic -5/3 exponent at small scales (e.g. $E(k) \propto k^{-5/3}$; Kolmogorov (1941)) gives way to a two-dimensional -3 exponent at large scales (e.g. $E(k) \propto k^{-3}$; Charney (1971)) . Schertzer and Lovejoy (1985) proposed a very different paradigm that represents the full range of atmospheric scales, from the millimeter to the planetary, as being governed by a single theory of anisotropic turbulence. Here, motions are separable according to the direction of the flow, given that the gravitational force acts in only one direction, rather than the scale of the flow. The spectral exponents were theoretically predicted to be $-5/3$ in the horizontal and $-11/5$ in vertical.

The challenge observationally has been that aircraft measurements are most easily peformed along isobars where the exponents may differ from their isoheight counterparts. When calculated along isobars, both paradigms predict a transition in the spectral exponent from $-5/3$ to some larger value at scales of hundreds of kilometers. For quasi-geostrophic turbulence, the large-scale isobaric exponent is -3 (Charney 1971), while for Lovejoy-Schertzer turbulence, it is -2.4 (Lovejoy et al. 2009).

The question of which paradigm is best supported by observed isobaric spectra has been the subject of considerable debate (Lovejoy et al. 2009; Lindborg et al. 2010; Frehlich and Sharman 2010; Schertzer et al. 2012). Although there is a consensus that some type of transition is present (Nastrom and Gage 1983; Nastrom et al. 1984; Nastrom and Gage 1985; Gao and Meriwether 1998; Cho and Lindborg 2001; Wiin-Nielsen 1967; Julian et al. 1970; Boer and Shepherd 1983), a quantitative analysis that includes a statistical fit to observations is rarely performed, and so it is not possible to conclusively discriminate which theory more closely reflects the true nature of turbulence. Beyond this isobaric debate, the Lovejoy-Schertzer paradigm has been almost entirely overlooked. Setting aside studies by the authors who originated the idea (Lovejoy et al. 2007; Pinel et al. 2012), the key prediction of the directional dependence of the exponent has not been tested – despite it having been proposed 40 years ago.

Fundamentally, the dichotomy is between two very different conceptual understandings of how air moves in the atmosphere. The commonly assumed transition paradigm argues that the dynamics are governed by physics that depends on spatial scale, whereas the Lovejoy-Schertzer paradigm proposes a single dynamical mechanism that governs atmospheric dynamics regardless of spatial scale. If the atmosphere can be shown to obey Lovejoy-Schertzer scaling, the tantalizing possibility is offered that observations at one scale and a simple scaling transformation may be all that is necessary to model atmospheric motions at all scales. Determining which paradigm is most closely reflected by observations is the goal of the study presented here.

Because the details are not widely known, in Sect. 2 we provide an overview of the theory behind Lovejoy-Schertzer turbulence as well as the various scale-dependent alternatives. Using multiple dropsonde and radiosonde datasets described in Sect. 3, we test the theoretical predictions made by both paradigms in Sect. 4. We consider a wide range of scales ranging from 200 m to 20,000 km with emphasis placed on careful examination of spectra calculated along both the horizontal and vertical directions, the directional dependence being the distinctive prediction of Lovejoy-Schertzer turbulence.

2. Theories of isotropic and anisotropic atmospheric turbulence

In general, turbulence laws serve to constrain how kinetic energy is distributed across spatial scales. Although these are most commonly represented through the power spectrum $E(k)$ of wind velocities as a function of the wavenumber k, there are other methods for performing a scale decomposition. Here, we consider the "structure function" as it is more robust to irregularly spaced sonde data (Lovejoy et al. 2007). The structure function may be thought of as a real space version of the wavenumber spectrum where k is replaced by a separation vector $\mathbf{\Delta r}$ of variable length and direction. Turbulence laws often hold for individual components of the wind vector $\mathbf{v}$, but for simplicity here we only consider the squared magnitude of the vector differences

$$\Delta v^2 \equiv (\mathbf{v}(\mathbf{r}) - \mathbf{v}(\mathbf{r}+\mathbf{\Delta r}))^2 . \tag{1}$$

Equation 1 is very general and it points to two basic questions.[1] First, how do the statistics of Δv^2 depend on the length of the separation vector $\mathbf{\Delta r}$? Second, how do the statistics of Δv^2 depend

[1] A third basic question is how do the statistics of Δv^2 depend on the spatial location $\mathbf{r}$? The turbulence theories considered in Table 1 assume translational invariance, i.e. that any statistics do not depend on location. Translational invariance is unlikely in the atmosphere due to, for example,

on the direction of $\mathbf{\Delta r}$? The answer to the second question of separation *direction* is the main subject of this paper. Many of the foundational theories, such as those proposed by Richardson, Kolmogorov, and Obukhov, assume that turbulence statistics are isotropic, or that there is no directional dependence for the statistics of the flow. Before addressing the alternative, anisotropic turbulence, we must first consider how the statistics vary as a function of separation *distance*.

Common to nearly all turbulence laws is the property of "scale invariance", which requires that fluctuations, when averaged over many potential realizations of the flow, follow a power-law function with respect to separation distance $\Delta r \equiv |\mathbf{\Delta r}|$ such that

$$\langle \Delta v^2 \rangle = \varphi \Delta r^{2H} \tag{2}$$

where H is a constant termed the Hurst exponent, and φ is some dimensionally relevant quantity that is conserved throughout the turbulent "cascade" from one scale to the next. Note that the kinetic energy spectrum in wavenumber space is obtained from Eqn. 2 via a Fourier transform to convert the real-space Δx into wavenumber k (Lovejoy and Schertzer 2013). The kinetic energy spectrum then becomes $E(k) \propto k^{-(2H+1)}$.

The next step is to identify the physical quantity φ that is conserved during the turbulent cascade. This is the primary aspect by which various theories of turbulence are distinguished. We consider four theories. The first and most widely known was proposed by Kolmogorov (1941) where the relevant cascade quantity is the kinetic energy dissipation rate ε, with units of energy per mass per time ($\mathrm{m}^2/\mathrm{s}^3$). This theory is also known as "three-dimensional" turbulence because, in its most basic form, it assumes isotropy, or that the statistics of the flow are identical in all three directions.

Three-dimensional turbulence has limited relevance for atmospheric motion given that it neglects buoyancy forces. The second theory we consider, proposed independently by Bolgiano (1959) and Obukhov (1959), addresses this concern by supposing the conserved cascading quantity relates to buoyancy forces rather than kinetic energy. For a Boussinesq flow, it can be shown that the conserved cascade quantity becomes $\phi = \partial f^2/\partial t$ where f is thermal buoyancy (Lovejoy and Schertzer 2013). The quantity ϕ is the "buoyancy variance flux" with dimensions of acceleration squared per time ($\mathrm{m}^2/\mathrm{s}^5$).

---

the altitude and latitude dependence of large scale dynamic features such as the jet stream. Here, we only consider velocity increments averaged over many spatial locations.

Bolgiano and Obukhov's theory was not widely adopted, and it was eventually replaced by various approaches based on the basic assumption that any feedback between the flow and the stratification is negligible. In these theories, stratification can influence the flow but the flow cannot modify the stratification–an idea encapsulated by the term "background" stratification. To this end, the third theory we consider here was proposed by Charney (1971) who adapted the theory of "two-dimensional" turbulence (Kraichnan 1967) to the atmosphere. Traditional two-dimensional turbulence holds that the conserved cascade quantity is "enstrophy flux" χ with units vorticity squared per time (s^{-3}). However, this theory was originally applied only to flows restricted to a plane such as a soap film. Charney modified the theory to account for some limited vertical flow, although the dominant set of dynamics remain a horizontal two-dimensional enstrophy cascade.

The original justification for neglecting feedbacks between the flow and stratification came from gravity wave theory, and so it is not surprising that gravity waves were later adopted directly to explain observed kinetic energy spectra, this time along the vertical direction (VanZandt 1982; Dewan 1997; Lindborg 2006). In this fourth theory, the wave frequency, termed the Brunt-Väisälä frequency N with units s^{-1}, takes the place of the conserved cascade quantity. Although N is not a typical cascade quantity, it nonetheless serves as the dimensionally relevant parameter for arguments based on dimensional analysis.

For all the above theories, specification of the relevant cascade quantity is sufficient to determine the value of the Hurst exponent H. The value of H is also the main testable prediction that can be used to discriminate between the various theories. Simply by using dimensional analysis, the kinetic energy fluctuation becomes a function of the relevant conserved cascade quantity φ and the separation distance r. In this case, dimensional consistency requires, respectively,

$$\langle \Delta v^2 \rangle = \varepsilon^{2/3} \Delta r^{2H}, \qquad H = 1/3 \qquad \text{(Kolmogorov spectrum)} \tag{3}$$

$$\langle \Delta v^2 \rangle = \phi^{2/5} \Delta r^{2H}, \qquad H = 3/5 \qquad \text{(Bolgiano-Obukhov spectrum)} \tag{4}$$

$$\langle \Delta v^2 \rangle = \chi^{2/3} \Delta r^{2H}, \qquad H = 1 \qquad \text{(Kraichnan spectrum)} \tag{5}$$

$$\langle \Delta v^2 \rangle = N^2 \Delta r^{2H}, \qquad H = 1 \qquad \text{(Gravity wave spectrum)} \tag{6}$$

Visually, the value of H imparts a unique character to any given transect or profile of v. A larger value of H implies a smoother profile, as illustrated in Fig. 1.

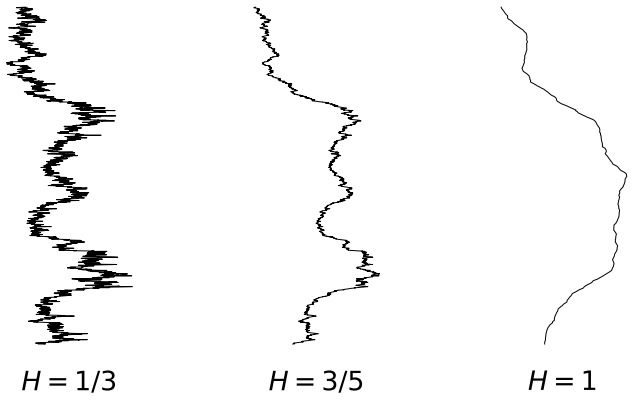

FIG. 1. Simulations of a mathematical stochastic process with varying H (cite scaleinvariance), representing example wind profiles that might be observed in hypothetical atmospheres where the theories represented by Eqns. 3-6 apply. The profiles are generated with the same random seed but have varying degrees of "smoothness" as specified by the value of H.

With respect to the directional dependence of the statistics defined by Eqn. 2, the simplest case is isotropy, where the statistics are identical for all directions of $\mathbf{\Delta r}$. However, it might instead be expected that the statistics of Δv^2 vary with direction in the atmosphere given that gravitational stratification has a strong directional dependence. In this case, it is conceivable that multiple theories could hold, even for the same spatial scale.

One such proposal, first made by Schertzer and Lovejoy (1985), considers that gravity, and therefore buoyancy, operate only in the vertical direction, and so the Bolgiano-Obukhov law (Eqn. 4) is likely to hold only in the vertical direction. Horizontally, the flow is not bound to a quasi-two dimensional layer as the Kraichnan law requires, so the horizontal statistics are likely to follow the Kolmogorov law (Eqn. 3):

$$\begin{cases} \langle \Delta v^2(\Delta x) \rangle \equiv \langle \Delta v(|\mathbf{\Delta x}|)^2 \rangle = \varphi_h \Delta x^{2H_h}, & \varphi_h = \varepsilon^{2/3}, \qquad H_h = 1/3, \\ \langle \Delta v^2(\Delta z) \rangle \equiv \langle \Delta v(|\mathbf{\Delta z}|)^2 \rangle = \varphi_v \Delta z^{2H_v}, & \varphi_v = \phi^{2/5}, \qquad H_v = 3/5, \end{cases} \tag{7}$$

where $\mathbf{\Delta x}$ represents a purely horizontal separation vector and $\mathbf{\Delta z}$ represents a purely vertical one. There is no distinction made between the two horizontal directions in this theory, and so $\mathbf{\Delta x}$ points in any horizontal direction. Together, we term Eqn. 7 the "Lovejoy-Schertzer" theory of turbulence.

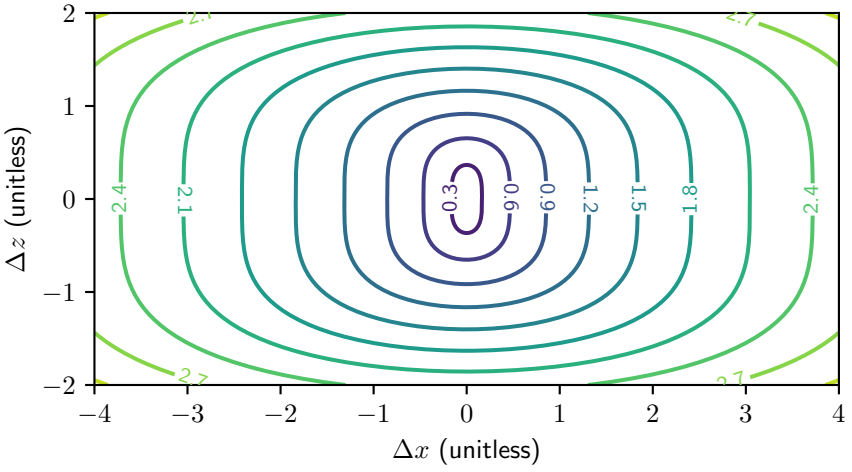

FIG. 2. Plot of the Lovejoy-Schertzer turbulent structure function (Eqn. 9), represent the average sizes, shapes, and strengths of turbulent circulations. The function is shown in nondimensional form, i.e. $\phi = \varepsilon = 1$, and the theoretical values $H_h = 1/3$ and $H_v = 3/5$. Note that the empirical structure functions plotted in Sect. 4 consider absolute values for Δx and Δz, which correspond to the first quadrant of this plot.

The two steps of dropping the isotropy assumption and proposing that two different laws hold simultaneously represent a significant shift from how turbulence is normally conceptualized.

It is worth considering the non-obvious implications of this conceptual shift in more detail. One way to view turbulence is as a spatial superposition of geometrically simple circulations of varying sizes and wind speeds. The turbulence laws Eqns. 3-5 may then be interpreted as a relationship between the cross-sectional length and the characteristic velocity of each of these simplified circulations. This picture works because the differences Δv used in the structure function effectively isolate the kinetic energy perturbations that are due to circulations of a particular size Δr. Thus, isolines of constant Δv^2 in $\Delta x, \Delta z$ space can be interpreted as describing the shapes and strengths of the simplified circulations from which the overall flow is "built". For the special case that turbulence is isotropic, the shapes of the circulations are spherical – any direction has identical statistics as any other direction. If the turbulence is anisotropic, then the circulations are no longer spherical, as is illustrated in Fig. 2.

In the Lovejoy-Schertzer theory of turbulence, the isolines are obtained by setting $\langle \Delta v^2(\Delta x) \rangle = \langle \Delta v^2(\Delta z) \rangle$ from Eqn. 7. Solving for the aspect ratios of the circulations, we obtain

$$\frac{\Delta x}{\Delta z} = l_s^{-4/5} \Delta z^{4/5}; \qquad l_s = \frac{\varepsilon^{5/4}}{\phi^{3/4}}. \tag{8}$$

Equation 8 is the first nontrivial implication of the Lovejoy-Schertzer theory. It implies that the mean aspect ratio of circulations systematically changes with circulation size (Fig. 2). Indeed, this scaling of aspect ratio with size aligns with our intuitive notion that large-scale atmospheric circulations such as the Hadley cell are highly elongated in the horizontal direction, whereas small-scale circulations such as small convective elements are more spherical or even elongated vertically. Because the aspect ratios systematically change with scale, there is a unique scale for which the aspect ratio is equal to unity and circulations are nearly spherical, termed the "spheroscale" l_s (Lovejoy and Schertzer 1985).

Another way to examine the shape of the turbulent circulations is to consider the full two-dimensional structure function $\langle \Delta v(\Delta x, \Delta z)^2 \rangle$. The simple requirement that $\langle \Delta v(\Delta x, \Delta z)^2 \rangle$ reduces to Eqns. 7 when $\Delta x = 0$ or $\Delta z = 0$ is not enough to specify a unique function. If we further require that isotropic turbulence is recovered when $H_h = H_v$ and $\varphi_v = \varphi_h$, then a unique function is specified, as shown in Fig. 2:

$$\langle \Delta v(\Delta x, \Delta z)^2 \rangle = \left(\varphi_h^{1/H_h} \Delta x^2 + \varphi_v^{1/H_h} \Delta z^{2H_v/H_h} \right)^{H_h}. \tag{9}$$

We now fit the two-dimensional structure function given by Eqn. 9 to observed wind statistics, allowing for both exponents H_v and H_h, as well as the coefficients φ_v and φ_h, to be determined empirically. With these four free parameters, Eqn. 9 becomes very general. It includes as special cases each of the theories for turbulence mentioned so far. An additional case worth mentioning is that the exponents are equal, but the constants φ_h and φ_v have different values. In this case, circulations have non-unitary aspect ratios but the aspect ratio does not change with circulation size. This type of anisotropy has been termed "trivial anisotropy" by Lovejoy and Schertzer (2013). Studies investigating turbulent anisotropy based on the anisotropy stress tensor limit themselves to trivial anisotropy if they assume the cascade remains controlled by kinetic energy with $H_h = H_v$,

TABLE 1. Various theories of atmospheric turbulence and corresponding parameter values for Eqn. 9. Here, N is the Brunt-Väisälä frequency, χ enstrophy flux, ϕ buoyancy variance flux, and ε kinetic energy flux. "Undefined" means that the parameter has no meaning within the context of the theory, while "not specified" indicates the parameter has some value but it is not specified by the theory. Note that Lindborg's theory (Lindborg 2006) suggests a transition between $H_v = 1$ to $H_v = 1/3$ at the Ozmidov length scale of order 3 m. Given that our measurements are at larger scales, we only consider the value $H_v = 1$.

Type	**Case**	**Exponents**	**Constants**
Isotropic	3D (Kolmogorov 1941)	$H_h = H_v = 1/3$	$\varphi_h = \varphi_v = \varepsilon^{2/3}$
	Bolgiano (1959); Obukhov (1959)	$H_h = H_v = 3/5$	$\varphi_h = \varphi_v = \phi^{2/5}$
	2D (Kraichnan 1967)	$H_h = 1$, H_v undefined	$\varphi_h = \chi^{2/3}$, φ_v undefined
	Gravity waves (VanZandt 1982)	$H_v = 1$, H_h not specified	$\varphi_v = N^2$, φ_h not specified
Anisotropic	Quasi-Geostrophic (Charney 1971)	$H_h = H_v = 1$	$\varphi_h = \chi_h^2, \varphi_v = \chi_v^2$, $\chi_v \ll \chi_h$
	Schertzer and Lovejoy (1985)	$H_h = 1/3, H_v = 3/5$	$\varphi_h = \varepsilon^{2/3}, \varphi_v = \phi^{2/5}$
	Lindborg (2006)	$H_h = 1/3, H_v = 1$	$\varphi_h = \varepsilon^{2/3}, \varphi_v = N^2$
	Anisotropic 3D	$H_h = H_v = 1/3$	$\varphi_h = \varepsilon_h^{2/3}, \varphi_v = \varepsilon_v^{2/3}$, $\varepsilon_h \neq \varepsilon_v$

as is sometimes done (Tennekes and Lumley 1972). Table 1 summarizes how Eqn. 9 relates to various turbulent theories.

3. Methods

We calculate structure functions from three datasets of wind velocity. The first contains dropsonde measurements from the ACTIVATE field campaign (Vömel et al. 2023), which took place over the North Atlantic Ocean between 2020 and 2022. Drops occurred during 169 flights spread over a variety of meteorological conditions and seasons. The second dropsonde dataset considered here was obtained from NOAA hurricane reconnaissance flights that took place between 1996 and 2012, mainly over the Gulf of Mexico and the Atlantic Ocean. Profiles were not considered if the data quality was marked as degraded or if the profile did not span the entire layer considered. We analyze a total of 683 ACTIVATE and 2325 hurricane profiles. Both dropsonde datasets contain vertical wind profiles $w(z)$ derived from the measured fall speed, the uncertainty in the measurements is of order $\sim 1\,\mathrm{m/s}$ (Wang et al. 2015; Vömel et al. 2023) – too large for the purposes of calculating a structure function. For this reason, we only consider structure functions calculated using horizontal

vector differences $\Delta v \equiv |\mathbf{v_h}(\mathbf{r}) - \mathbf{v_h}(\mathbf{r}+\mathbf{\Delta r})|$ where $\mathbf{v_h}$ is the horizontal component of the full wind vector $\mathbf{v}$.

The third dataset we consider is the horizontal wind data from the Integrated Global Radiosonde Archive (IGRA) (Durre et al. 2006), a composite created from global balloon-borne soundings obtained from thousands of stations and spanning many decades. A limitation of the dataset is that measurement methods and techniques vary temporally and spatially. For example, many modern sensors use GPS to measure geopotential height, but height inferred from pressure is also used, particularly for older data. Accordingly, we only consider measurements from the period between the years 2010 and 2025 when GPS data can be assumed to be in sufficiently widespread use. Measurement uncertainties for the two models of radiosonde widely used during this period, the Vaisala RS41 (Vaisala Oyj 2017; Dirksen et al. 2014) and the Graw DFM-17, (Graw Radiosondes GmbH & Co. KG 2024; Dirksen et al. 2014) are of order 10 m (geopotential height), 1 hPa (pressure), and 0.1 m/s (horizontal wind). The variety of measurement techniques used to compose the IGRA dataset introduces a source of uncertainty that is difficult to quantify, given that the techniques are not reported in the dataset. As an example, in Appendix A1 we show a near perfect split in calculated Hurst exponents based on sounding nationality, a result likely caused by processing techniques being standard within a country but differing between countries. Any uncertainties we report below should therefore be interpreted with significant caution.

Shear measurements calculated from radiosonde and dropsonde horizontal wind profiles also have uncertainties related to sonde inertia (Fig. 3). If a sonde passes between layers with different mean wind speeds, the sonde does not immediately adjust to the new wind speed due to its inertia. Since horizontal wind velocity is approximated by the velocity of the sonde itself, shear cannot be measured over any distance smaller than the distance over which the sonde adjusts to a different horizontal wind. To account for this adjustment scale, and to remove additional spurious high-frequency wind variability due to e.g. oscillations caused by the payload swinging underneath the balloon, a smoothing is commonly applied to the wind profiles during data processing. The smoothing applied to ACTIVATE and hurricane sondes had a timescale of 5 s (Vömel et al. 2023) and 10 s, (Durre et al. 2006) respectively, while a typical radiosonde smoothing timescale is 40 s (Dirksen et al. 2014). Therefore, assuming typical descent/ascent rates of 20 m/s (dropsondes; Vömel et al. (2023); Wang et al. (2015)) and 5 m/s (radiosondes; Dirksen et al. (2014)), the spatial

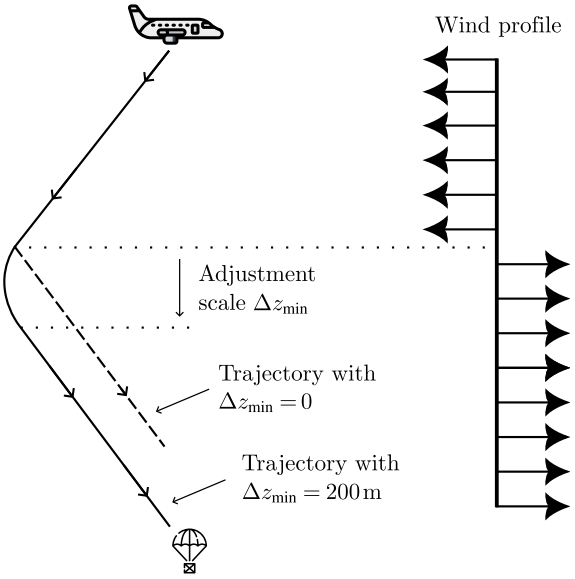

239 FIG. 3. Illustration of how dropsonde measurements of horizontal wind fluctuations $\Delta v(\Delta z)$ are effectively
240 smoothed by sonde inertia. Wind fluctuations that occur over a smaller spatial scale than the sonde's adjustment
241 scale $\Delta z_{\min}$ cannot be reliably measured.

237 scales for sonde adjustment are of order 200 m in both cases. We therefore limit our analysis of
238 vertical wind fluctuations to scales larger than $\Delta z_{\min} = 200\,\mathrm{m}$.

242 To obtain H in Eqns. 2 and 9, only second order structure functions are calculated here, although
243 structure functions of other orders have also been considered by other studies. For comparison
244 with prior results, we reproduce in the Supplement our analysis for first- and third-order structure
245 functions $\langle \Delta v \rangle$ and $\langle \Delta v^3 \rangle$, respectively. All structure functions are calculated from all possible
246 point pairs within a given profile, time period, or region, and fitted values are obtained using a least-
247 squares regression. Uncertainties are reported as 95% confidence intervals for the least-squares
248 fit and do not include systematic uncertainties originating from processing methodologies such as
249 dataset smoothing.

250 For the IGRA data set, the structure functions are calculated for both vertical and horizontal
251 separation directions. Purely vertical structure functions are calculated from individual sondes,
252 each released for the 00z and 12z launch times between 2010 and 2025. Structure functions
253 calculated along the horizontal direction are obtained using observations from different devices,
254 first by identifying nearly simultaneous sonde launches. Then, each point observation is paired

with each other point observation to obtain a list of observation pairs with varying horizontal and vertical separations. To be included in the analysis, observation pairs are required to have taken place within 2 hours of each other. For one-dimensional structure functions calculated along the horizontal direction, observations are also required to have vertical separations no larger than 50 m. Due to the volume of data, it is not possible to consider all observation pairs from all possible sounding launches, and so only soundings launched at 00z or 12z from every tenth day between 2010 and 2025 are considered for any structure function calculated along the horizontal direction.

a. Effect of non-instantaneous sonde measurements

Here, we ignore temporal variability in the statistics for turbulent wind fluctuations in order to isolate the spatial statistics as given by Eqn. 7. However, the sondes do not, in fact, measure wind profiles instantaneously. Dropsondes obtain profiles over approximately one hour, while radiosondes require two to three hours.

To estimate whether time differences between observation pair measurements impact our analyses, consider that, for isotropic turbulence, a turbulent circulation of size l has a lifetime of order $\tau \sim l/\Delta v$ where Δv is the wind speed associated with the circulation. For the spatial statistics of the circulation to be accurately sampled, the sonde must cross the circulation within a time interval that is shorter than the circulation lifetime. For sonde velocity V, this requires $l/V < \tau$ or equivalently $V > \Delta v$, implying that the sonde can only measure turbulent velocity fluctuations of a magnitude smaller than the sonde velocity. Given that dropsondes with vertical velocities between 15 and 20 m/s satisfy this condition for most of the measured range of scales, and that their measurements also support anisotropy, this isotropic criterion is less relevant.

For an anisotropic circulation, the horizontal and vertical circulation sizes are not identical, and the circulation's lifetime must be estimated using its horizontal length given that we are considering horizontal velocity components. In this case, accurate measurements of the vertical profile require $V > v l_z/l_x$ where l_z is the vertical circulation length or the distance the sonde must pass through to sample a single eddy circulation. From Eqn. 8, large eddies are most anisotropic with aspect ratios $l_z/l_x \ll 1$. The largest measured velocity difference among spatially separated measurements in the dataset is $\sim 20\,\mathrm{m/s}$, associated with eddies that are the most stratified with the smallest values of l_z/l_x according to Eqn. 8. These velocity differences are nonetheless only approximately four times

faster than the slowest sonde velocity of 5 m/s (for the radiosondes). The sonde measurements may therefore be assumed effectively instantaneous.

We also include in our analysis horizontally separated measurement pairs that are separated in time by up to two hours. A typical circulation of horizontal size l_x has a typical lifetime of $\tau = l_x/\Delta v$ where Δv is the wind speed associated with the circulation. The minimum distance in our horizontal measurement pairs is set to 2×10^5 m, so that the minimum circulation lifetime is of order $\tau = 2 \times 10^5\,\mathrm{m}/10\,\mathrm{m/s} = 2 \times 10^4$ s, or about 5.5 hours, implying that observation pairs separated by a maximum of two hours may be considered effectively instantaneous. As a final check that this two-hour threshold is sufficient, we also computed a one-dimensional horizontal structure function for observation pairs that had vertical separations less than 5 m and were taken within 5 min of each other (see Supplement S3). Results for both sets of thresholds (5 m, 5 min) and (50 m, 120 min) indicated Hurst exponents that were nearly identical.

4. Results

First, we evaluate the structure function along the vertical direction (Eqn. 7) for the lowest 8 km of the atmosphere, which is the layer measured by both dropsonde datasets and IGRA radiosondes. As shown in Fig. 4, the structure functions closely follow a power-law relationship over the full range of observed scales $0.2\,\mathrm{km} \leq \Delta z \leq 8\,\mathrm{km}$. Calculated values of H_v range from 0.513 ± 0.008 for IGRA to 0.71 ± 0.01 for ACTIVATE.

To investigate the dependence of the vertical Hurst exponent with height, wind measurements are divided into layers of thickness 2 km. A Hurst exponent H_v is calculated for the vertical structure function for Δz ranging between 0.2 km and 2 km for each layer. Fig. 5 highlights how the calculated Hurst exponents lie close to the Lovejoy-Schertzer predicted value at each level within the troposphere. Full structure functions as in Fig. 4 but for each layer are provided in the Supplement. Above an altitude of roughly 18 to 20 km, H_v decreases to a value lying between approximately 0.4 and 0.5, which does not agree with any of the theories for turbulence described in Tab. 1. As shown in the Supplement, tropospheric Hurst exponents for first- and third-order structure functions ($\langle \Delta v \rangle$ and $\langle \Delta v^3 \rangle$, respectively) are also consistent with the Lovejoy-Schertzer prediction.

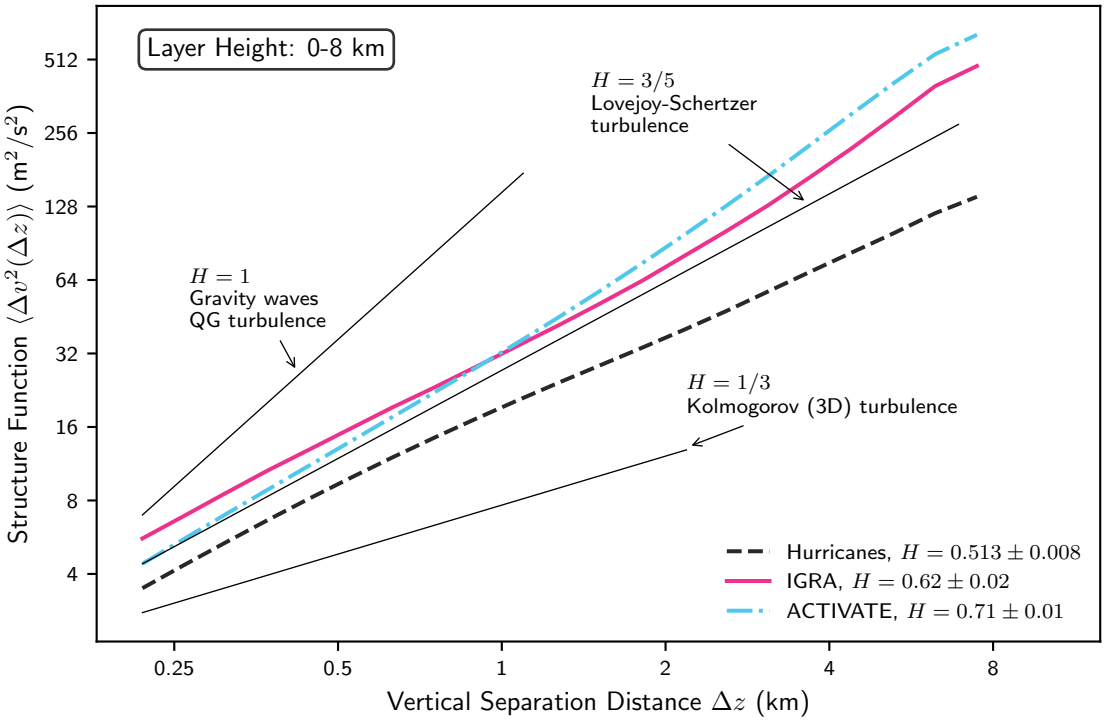

FIG. 4. Vertical structure functions for the IGRA (pink solid), the NOAA hurricane dropsonde dataset (black dashed) and the ACTIVATE dropsonde dataset (blue dot-dashed). Structure functions and Hurst exponents (Eqn. 2 are calculated for the lowest 8km of the troposphere, which is the layer measured by all three datasets.

Horizontal structure functions $\langle \Delta v(\Delta x) \rangle$ calculated using IGRA data are shown in Fig. 6. There data show clear power-law behavior for separations smaller than about 1800 km, while for larger scales the Hurst exponent approaches 0 between approximately 3000 km and the planetary half-circumference of 20000 km. Regressions to the steepest portion of the slope between 200 km and 1800 km indicate a value for H_h of 0.50 ± 0.02.

a. Two-dimensional structure functions

Different values of the vertical and horizontal Hurst exponents supports the view that atmospheric turbulence is non-trivially anisotropic, specifically that the aspect ratios of atmospheric circulations may systematically change with scale as implied by Eqn. 8. To address this possibility, we now examine in detail the full two-dimensional structure functions represented by Eqn. 9. Note that Eqn.

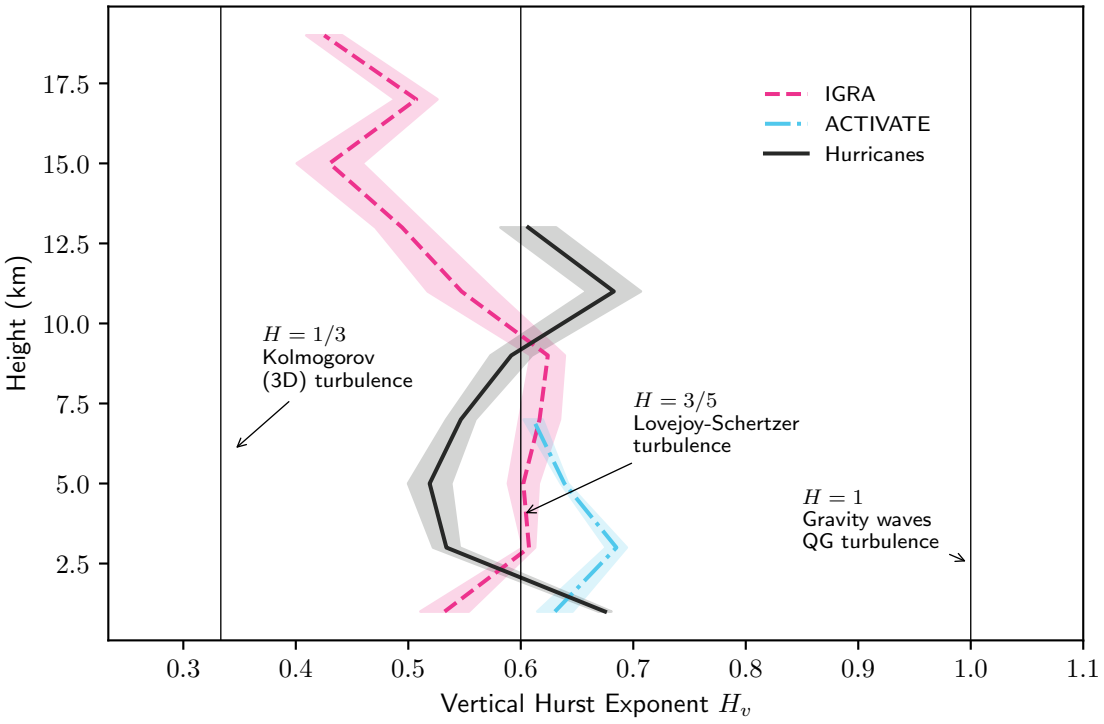

315 FIG. 5. Hurst exponents and 95% confidence calculated for structure functions as shown in Fig. 4 but evaluated
316 within stacked layers 2 km thick.

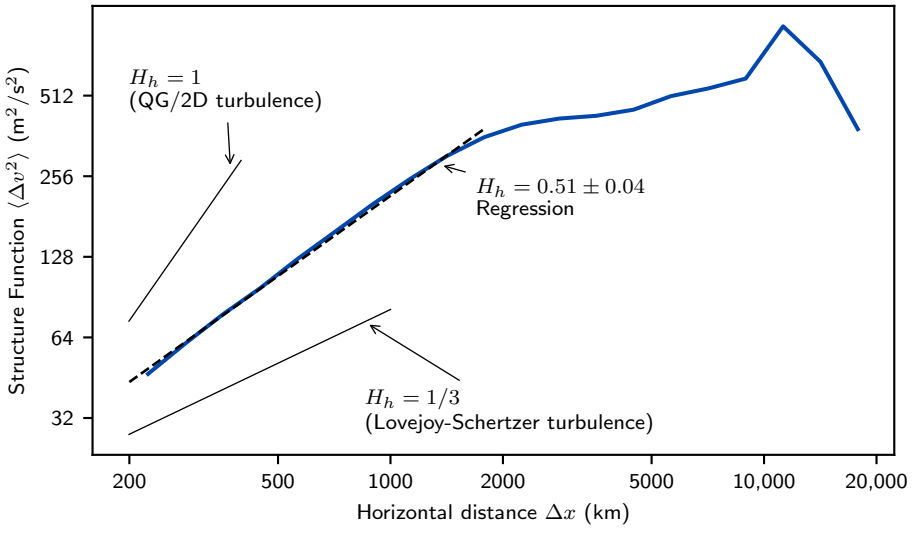

322 FIG. 6. Horizontal structure function $\langle \Delta v \rangle (\Delta x)$ calculated from IGRA radiosonde data and the associated
323 theoretical power-law relationships for different turbulence theories shown in Table 1.

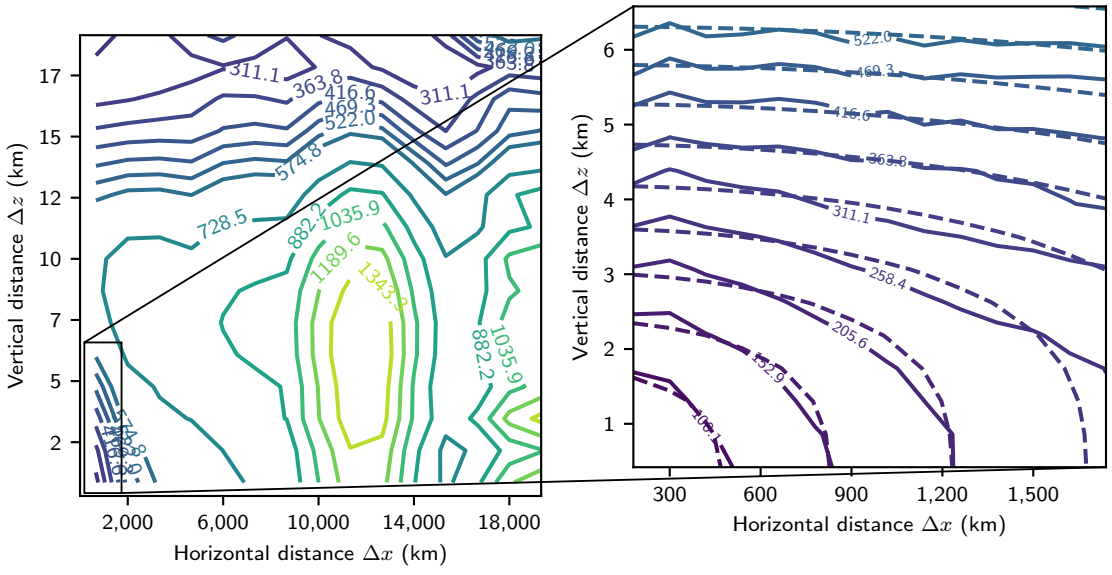

FIG. 7. Empirical two-dimensional horizontal/vertical structure function calculated from IGRA radiosonde data (solid; labels in m^2s^{-2}). For the inset, a fit (dashed) was performed using Eqn. 9, with best-fit parameters described in text.

9 cannot be easily logarithmically transformed, so what follows is limited to analyses calculated in linear space.

Fig. 7 shows the empirical two-dimensional structure function $\langle \Delta v(\Delta x, \Delta z) \rangle$ plotted for two ranges of scale. As was also seen in Fig. 6, the largest scales up to 20000 km horizontally and 20 km vertically show no clear power-law dependence of Δv on Δx, indicative of a regime that is not dominated by any turbulence theory listed in Table 1. By contrast, at horizontal separations between 200 km and 1800 km, and for vertical separations smaller than 7 km, the empirical structure function is well approximated by a least-squares fit to Eqn. 9, with empirical values $H_h = 0.37 \pm 0.01$, $H_v = 0.63 \pm 0.01$, $\varphi_h = 0.08 \pm 0.01\,\mathrm{m}^{2-2H_h}\mathrm{s}^{-2}$, and $\varphi_v = 0.092 \pm 0.009\,\mathrm{m}^{2-2H_v}\mathrm{s}^{-2}$.

From Eqn. 8 and the theoretical relations $\varphi_h = \varepsilon^{2/3}$ and $\varphi_v = \phi^{2/5}$ (Tab. 1), empirical values for φ_h and φ_v imply a spheroscale of order 1m. Values calculated for H_h and H_v are nearly consistent, whether they are calculated from the two-dimensional structure functions shown in Fig. 7 or from the one-dimensional structure functions shown in Figs. 4-6.

Although we are unaware of any theory that predicts different Hurst exponents for the two horizontal directions, for completeness a two-dimensional structure function for the zonal (x) and meridional (y) directions is calculated from the sounding observations as shown in Fig. 8. The

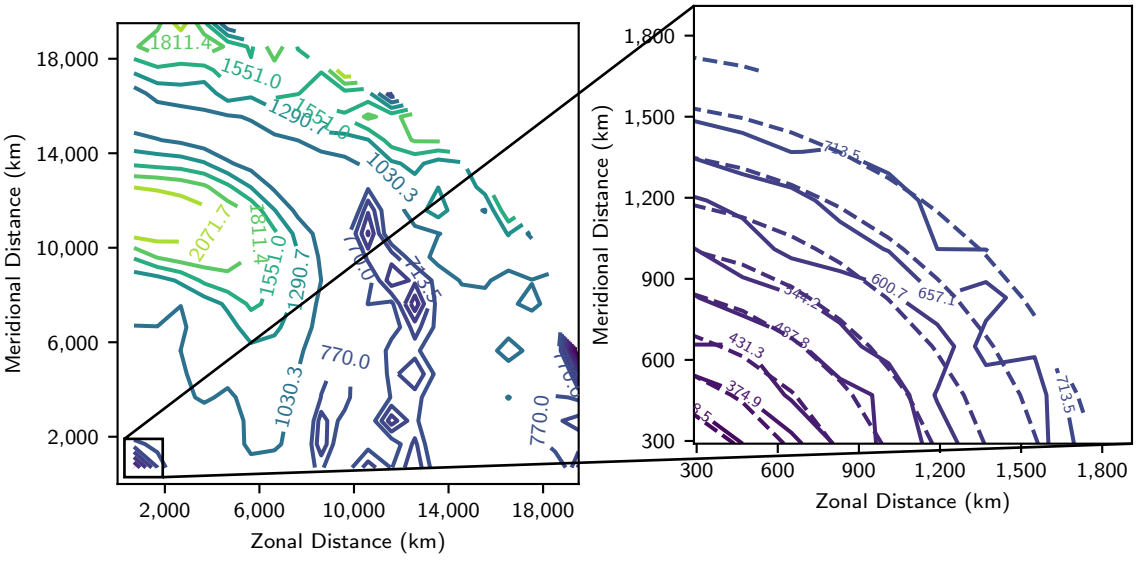

FIG. 8. As shown in Fig. 7, but for isoheight statistics calculated as a function of meridional and zonal direction.

structure function displays a maximum in Δv^2 near $\Delta x \sim 0$ and $\Delta y \sim 10{,}000\,\mathrm{km}$, which might be speculated to correspond to the jet stream. Otherwise, there is a "flattening" with $H_h \to 0$ at horizontal separation scales larger than $\sim 1800\,\mathrm{km}$ as in Fig. 6.

For separations smaller than $\sim 1800\,\mathrm{km}$, the empirical structure function is fit to a functional form that is analogous to Eqn. 9 but that applies in the x and y two horizontal directions:

$$\langle \Delta v(\Delta x, \Delta y)^2 \rangle = \left(\varphi_x^{1/H_x} \Delta x^2 + \varphi_y^{1/H_x} \Delta y^{2H_y/H_x} \right)^{H_x} . \tag{10}$$

Values for the least-squares fit are $H_x = 0.35 \pm 0.05$, $H_y = 0.33 \pm 0.03$, $\varphi_x = 0.17 \pm 0.11\,\mathrm{m}^{2-2\mathrm{H_x}}\mathrm{s}^{-2}$, and $\varphi_y = 0.23 \pm 0.10\,\mathrm{m}^{2-2\mathrm{H_y}}\mathrm{s}^{-2}$. These values are consistent with the turbulence being either horizontally isotropic or "trivially anisotropic", with $H_x \simeq H_y$ but $\varphi_x \neq \varphi_y$, as noted also by Lovejoy and Schertzer (2011) based on an examination of reanalysis datasets. We find a mean aspect ratio for circulations of $\varphi_x/\varphi_y = 0.75 \pm 0.60$.

5. Discussion

For structure functions calculated along the vertical direction, the prediction of the prevailing "transition" paradigm is that $H_v = 1$ for the largest vertical scales, whether the model is a quasi-two-dimensional enstrophy cascade (Charney 1971) or gravity waves (Dewan 1997). At smaller

scales there is a transition to Kolmogorov turbulence where $H_v = 1/3$ (Lindborg 2006). Neither value of H_v is supported by Figs. 4 and 5, at least for vertical separations down to 200 m.

It is especially notable that the Kolmogorov value of $H_v = 1/3$ is not supported even within the boundary layer below 2 km in altitude (Fig. 5). This challenges the prevailing viewpoint that Kolmogorov turbulence, in either its isotropic or anisotropic forms (Table 1), characterizes kilometer-scale boundary layer turbulence. If Kolmogorov turbulence does apply to the boundary layer, Fig. 5 suggests that it can only exist for vertical separation scales smaller than 200 m that are not resolved here.

For large-scale structure functions calculated along the horizontal direction (Fig. 6), the calculated value of $H_h = 0.50 \pm 0.02$ is a little higher than the $H_h = 1/3$ value predicted by Lovejoy-Schertzer turbulence. Nonetheless, it lies closer to 1/3 than the value of $H_h = 1$ expected for a two-dimensional turbulent enstrophy cascade as suggested by Charney (1971) and Nastrom and Gage (1983), and therefore these results also appear to invalidate the transition paradigm.

Overall, Hurst exponents for both the horizontal and vertical separation directions appear more strongly supportive of the Lovejoy-Schertzer paradigm of stratified turbulence (Eqn. 7) than the transition paradigm. The two dimensional structure function $\Delta v(\Delta x, \Delta z)$ (Fig. 7) provides what is perhaps the most compelling support as it is not restricted to the orthogonal horizontal and vertical directions and therefore was calculated using many more observation pairs. A fit using Eqn. 7 approximately reproduces the empirical isolines of constant Δv, and the best-fit exponent values $H_h = 0.37 \pm 0.01$, $H_v = 0.63 \pm 0.01$ are again close to the theoretical values predicted by the Lovejoy-Schertzer theory of turbulence of $H_h = 1/3$ and $H_v = 3/5$.

a. The effect of vertical smoothing on the Hurst exponents

The largest discrepancy between the empirically derived exponents obtained here and those predicted by the Lovejoy-Schertzer theory of turbulence is the value $H_h = 0.50 \pm 0.02$ obtained from the one-dimensional horizontal structure function in Fig. 6. In fact, it does not clearly match any of the turbulence theories shown in Table 1.

The discrepancy is reminiscent of the isobaric spectrum controversy discussed in the introduction – even if $H = 1/3$ along isoheights it is possible that $H > 1/3$ along isobars. Lovejoy et al. (2009) argued that the basic reason that isobaric and isoheight structure functions differ is that isobars

gently slope over large horizontal distances. As an example consider a sloping trajectory where $\Delta z = c\Delta x$. In this case, from Eqn. 9, the observed structure function would follow

$$\langle \Delta v(\Delta x)^2 \rangle = \left(\varphi_h^{1/H_h} \Delta x^2 + \varphi_v^{1/H_h} (c\Delta x)^{2H_v/H_h} \right)^{H_h}. \tag{11}$$

Given that $H_v/H_h > 1$ (Fig. 7), at small scales the Δx^2 term dominates so that the observed structure function scales as $\langle \Delta v(\Delta x)^2 \rangle \sim \Delta x^{2H_h}$, while at larger scales the $\Delta x^{2H_y/H_x}$ term dominates so that $\langle \Delta v(\Delta x)^2 \rangle \sim \Delta x^{2H_v}$. The implication is that a sloping trajectory will transition from $H \approx 1/3$ at smaller scales to $H \approx 3/5$ at scales of roughly hundreds of kilometers. This transition scale is consistent with the well-known spectrum observed by Nastrom and Gage (1983) that helped motivate acceptance of the transition paradigm.

Crucially, the implication is that any observed large-scale isobaric Hurst exponent cannot be simply assumed to be equal to the large-scale isoheight Hurst exponent, even though isobars are nearly flat. The more general lesson is that $H_h > 1/3$ can be observed in the large-scale horizontal structure function if the observations depart even slightly from lying on a perfect isoheight surface.

Although our isoheight measurements are not isobaric, there is reason to believe that they also do not represent perfectly horizontal separations, mainly because radiosonde measurements are smoothed over a characteristic vertical distance of order $\sim 200\,\mathrm{m}$. [2] Smoothing implies that a wind measurement at a given height is a function of the wind at nearby heights, plausibly causing vertically-separated fluctuations to influence any calculated horizontally-separated fluctuations. As a note, such smoothing cannot necessarily be removed by simply reprocessing the data. All sondes have a finite timescale of adjustment to the local wind in the presence of vertical wind shear. Such a timescale introduces an effective smoothing regardless of how the data are processed.

To investigate the effect of vertical smoothing on horizontal statistics, we performed an experiment in a numerical hydrodynamic simulation using the System for Atmospheric Modeling (Khairoutdinov and Randall 2003). The simulation is of a tropical atmosphere and uses a numerical grid with 100 m spacing along all three directions in the layer where we performed our analysis, which was between 2 and 10 km. The domain size is $204\,\mathrm{km} \times 204\,\mathrm{km}$. Details of the simulation are provided in Dazlich et al. (2013).

[2] A second reason measurements may not represent perfect isoheights is measurement error in the vertical location, which would also tend to "smooth" the mean statistics in a similar manner. But given that measurement uncertainty in the GPS radiosondes is of order $\sim 10\,\mathrm{m}$, we assume vertical smoothing due to sonde inertia is more important.

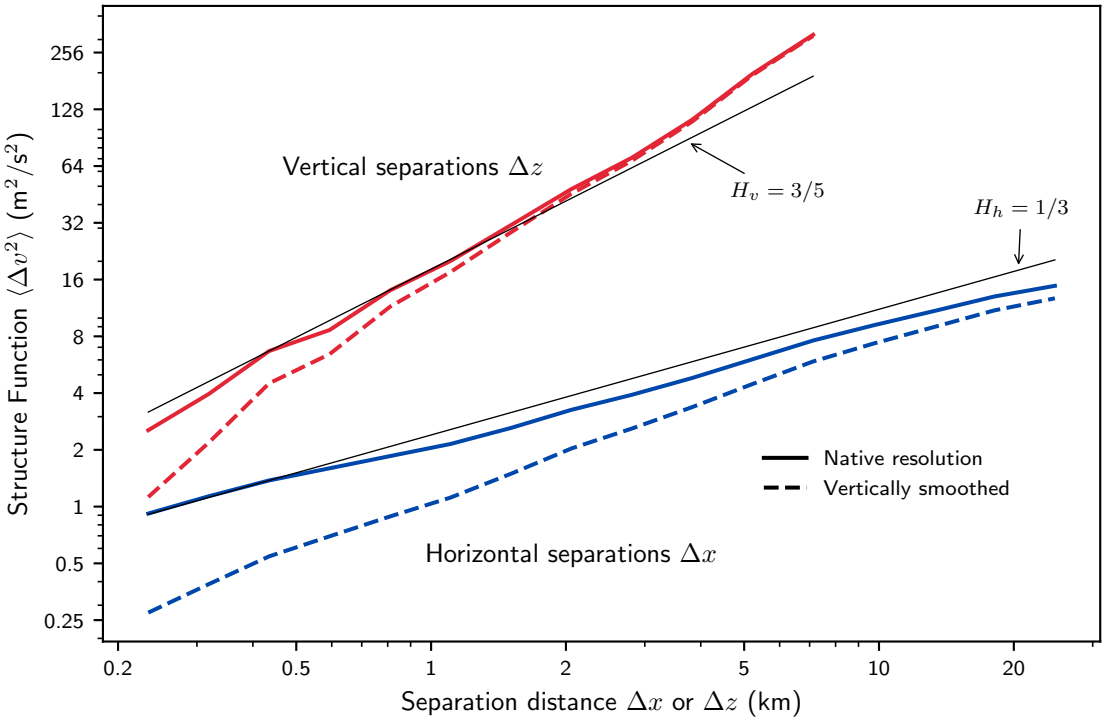

FIG. 9. Vertical (red) and horizontal (blue) structure functions calculated for the SAM simulation. Fitted values for the exponents are $H_h = 0.37 \pm 0.01$ and $H_v = 0.75 \pm 0.02$ at native resolution (solid). When the wind field is smoothed vertically prior to calculating structure functions, both exponents increase to $H_h = 0.49 \pm 0.01$ and $H_v = 0.84 \pm 0.02$ (dashed). The theoretical values $H_h = 1/3$ and $H_v = 3/5$ according to Lovejoy-Schertzer theory are shown for reference (thin black).

Vertical and horizontal structure functions calculated for SAM at its native resolution lie close to the Lovejoy-Schertzer scaling (Fig. 9). Omitting separation distances equal to one grid point, which may be more affected by numerical artifacts, calculated Hurst exponents for SAM are $H_v = 0.69 \pm 0.02$ and 0.305 ± 0.008. As anticipated, when vertical smoothing is applied using a vertical Gaussian convolution with a standard deviation of two grid points or 200 m, the horizontal Hurst exponent increases to $H_h = 0.42 \pm 0.01$. The vertical Hurst exponent is also increased to a value $H_v = 0.79 \pm 0.03$. Notably, smoothing is only performed along the vertical direction but the horizontal Hurst exponent is nonetheless strongly affected.

Because the domain size is smaller than the horizontal measurements from IGRA, the result that vertical smoothing increases the horizontal Hurst exponent should be viewed as qualitative

rather than quantitative. More rigorous testing, perhaps with large-scale multifractal simulations with known Hurst exponents, would be necessary to determine whether the magnitude of the discrepancy between the IGRA-derived horizontal Hurst exponents and theory could be explained by vertical smoothing. Even so, Fig. 9 suggests that vertical smoothing may plausibly explain why observations of H_h are a little higher than expected by Lovejoy-Schertzer turbulence – without needing to invoke any new set of physics such as quasi-geostrophic turbulence.

We should note that applying a vertical smoothing directly to Eqn. 9 can only decrease, rather than increase, the calculated horizontal Hurst exponent H_h. The reason is that Eqn. 9 applies for mean values of Δv^2 that are averaged over many realizations of the flow. This implies that the full distribution of values for Δv^2, rather than simply the mean $\langle \Delta v^2 \rangle$, must be considered to fully explain why H_h is higher due to vertical smoothing. This is in contrast to the isobaric mechanism explanation for bias in measurements of H_h suggested by Lovejoy et al. (2009), where the increase of H_h may be derived directly from the mean statistics for Δv^2 represented by Eqn. 9 using the argument shown above.

That the sounding data includes vertical smoothing may also explain Lovejoy et al. (2007)'s prior finding of an increase in H_v with altitude. Given that dropsondes such as those used by Lovejoy et al. (2007) have a faster fall speed in the upper troposphere (e.g. Vömel et al. 2023), a given dropsonde-wind shear adjustment timescale would imply upper-tropospheric measurements are effectively smoothed over a larger vertical spatial scale than lower-tropospheric measurements. If Hurst exponent calculations include scales affected by smoothing, a spurious altitude dependence of H_v could result. Lovejoy et al. (2007) included separations down to 5 m in their analyses, which is much smaller than our 200 m threshold and plausibly introduced a spurious dependence of H_v on altitude that is not seen in Fig. 5.

6. Conclusions

It is widely assumed that the dynamics of the atmosphere are controlled by a heirarchy of distinct dynamical mechanisms, each restricted to some limited range of spatial scales. The distribution of kinetic energy is thought to be determined by a quasi-two-dimensional enstrophy cascade at the largest scales (Charney 1971; Nastrom et al. 1984), gravity waves at the mesoscale (Dewan 1997; Lindborg 2006), and a three-dimensional turbulent energy cascade at the smallest scales (Tennekes

and Lumley 1972). Such a hierarchy would imply clear transitions in the Hurst exponents for kinetic energy structure functions when calculated along either the horizontal or vertical directions, from $H = 1$ at large scales to $H = 1/3$ at small scales.

Here, we use high-resolution dropsonde and radiosonde measurements to calculate structure functions for horizontal wind separated both horizontally and vertically. We find a Hurst exponent close to $H_v \approx 0.6$ for vertical separations between 200 m and 8 km, which is inconsistent with both small-scale isotropic turbulence and mesoscale gravity waves. Along the horizontal direction, large scale structure functions show a Hurst exponent with value $H_h \approx 0.4$ for separation scales ranging from 200 m to 2000 km, which is inconsistent with a large-scale enstrophy cascade. We argue that these measured structure functions are closely consistent with a lesser known theory of "Lovejoy-Schertzer" turbulence with $H_h = 1/3$ and $H_v = 3/5$ at all scales (Schertzer and Lovejoy 1985). We show that the small difference between the observed and Lovejoy-Schertzer value of H_h is plausibly due to vertical smoothing of radiosonde data.

Thus, we find that the canonical "transition" paradigm has little empirical support. Instead, it appears that the dynamics of the troposphere and most of the stratosphere are controlled by a single wide-ranging anisotropic turbulent cascade rather than a hierarchy of independent dynamical mechanisms. Looking forward, more measurements of structure functions or spectra as a function of separation direction will be necessary to confirm Lovejoy-Schertzer scaling. Scales smaller than 200 m, which were not resolved here, are of particular interest for determining whether small-scale turbulence is isotropic with $H_h = H_v$. Simultaneous wind observations separated in both the horizontal and vertical direction will be necessary for such an analysis. The extent to which vertical smoothing affects calculations of horizontally-separated structure functions could also be quantified, perhaps by considering multifractal simulations with known exponents (Lovejoy and Schertzer 2010).

Acknowledgments.

Data availability statement.

APPENDIX

A1. Vertical Hurst exponents for individual meteorological stations

Reported vertical Hurst exponents from the IGRA data were computed after the structure function was averaged over all available stations to obtain a global mean value of H_v. Here, we calculate the exponents for individual stations by identifying which stations contained at least 730 complete soundings, corresponding to at least two years. Then, mean structure functions and Hurst exponents were calculated for individual 2 km-thick vertical layers as in Sect. 4 and Fig. 5. Finally, we filtered the calculated exponents by requiring the 95% confidence interval of the least-squares fit to be less than 0.05, which ensures the assumption that the structure functions are scaling is reasonably accurate for the fitted structure functions. This filtering process resulted in a total of 366 stations for consideration.

Figure A1 shows the vertical Hurst exponents as a function of height for each IGRA station. Overall, a large majority of values are much closer to the Bolgiano-Obukhov value of 3/5 than the values of 1/3 or 1 that correspond to three-dimensional or two-dimensional turbulence, respectively. There also appears to be a bimodal distribution below 8 km, with a cluster of values near 0.6 and a cluster closer to 0.75. At first glance, this might indicate evidence of two separate turbulence regimes, possibly depending on latitude or some other climatological factor. However, we also observe a nearly perfect split between the two regimes based on sounding nationality. For example, for the layer between 4 km and 6 km, 83 out of 84 U.S.A.-based soundings had a Hurst exponent smaller than 0.63, whereas 79 out of 84 Hurst exponents measured from China-based soundings were larger than 0.66. Recall that the value of the exponent is sensitive to data processing methods, such as the period of the vertical smoothing applied to the raw data as shown in Sect. a. Since it is likely that the methods are uniform within a country but differ between different countries, the bimodal distribution in Fig. A1 is likely an indication of data processing artifacts rather than some dependence on local meteorology.

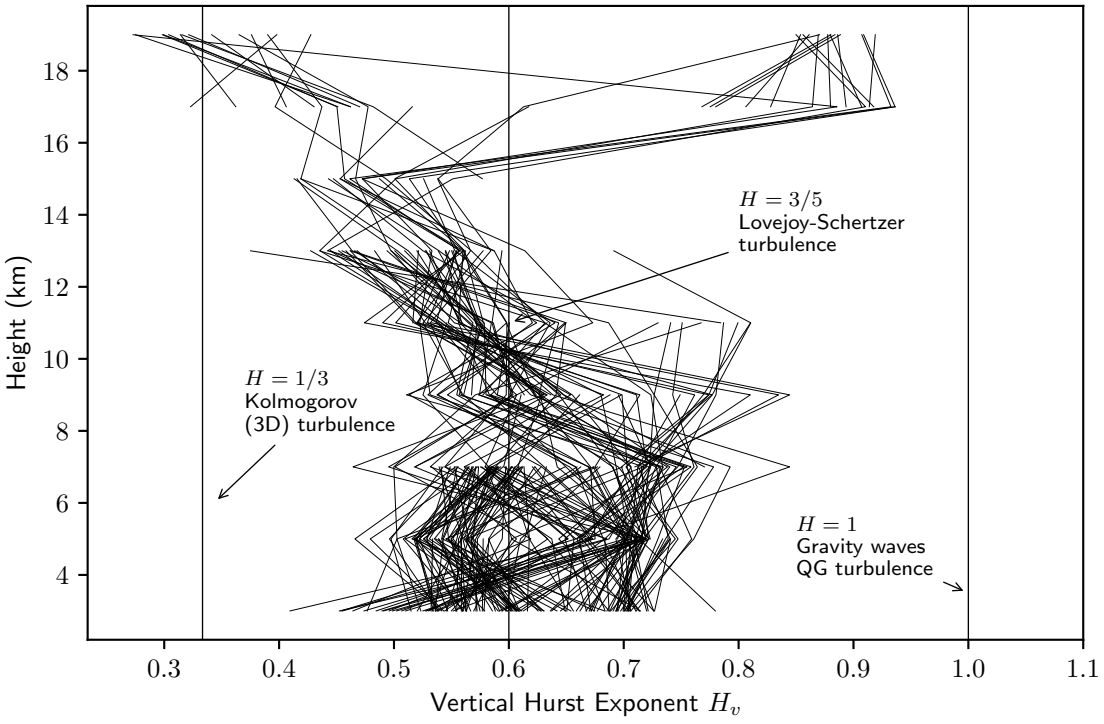

FIG. A1. As in Fig. 5, but for individual IGRA stations (thin black lines).

References

Boer, G. J., and T. G. Shepherd, 1983: Large-scale two-dimensional turbulence in the atmosphere. *Journal of Atmospheric Sciences*, **40 (1)**, 164 – 184, https://doi.org/10.1175/1520-0469(1983)040<0164:LSTDTI>2.0.CO;2.

Bolgiano, R. J., 1959: Turbulent spectra in a stably stratified atmosphere. *Journal of Geophysical Research (1896-1977)*, **64 (12)**, 2226–2229, https://doi.org/https://doi.org/10.1029/JZ064i012p02226.

Charney, J. G., 1971: Geostrophic turbulence. *Journal of Atmospheric Sciences*, **28 (6)**, 1087 – 1095, https://doi.org/10.1175/1520-0469(1971)028<1087:GT>2.0.CO;2.

Cho, J. Y. N., and E. Lindborg, 2001: Horizontal velocity structure functions in the upper troposphere and lower stratosphere: 1. observations. *Journal of Geophysical Research: Atmospheres*, **106 (D10)**, 10 223–10 232, https://doi.org/https://doi.org/10.1029/2000JD900814.

Dazlich, D., and Coauthors, 2013: The Giga-Large Eddy Simulation-2 Experiment. *CMMAP Team Meeting*, Ft. Collins, CO, Center for Multisc. Mod. of Atmos. Proc., https://hogback.atmos.colostate.edu/cmmap/research/docs/aug13/poster-don.pdf.

Dewan, E., 1997: Saturated-cascade similitude theory of gravity wave spectra. *Journal of Geophysical Research: Atmospheres*, **102 (D25)**, 29 799–29 817, https://doi.org/https://doi.org/10.1029/97JD02151.

Dirksen, R. J., M. Sommer, F. J. Immler, D. F. Hurst, R. Kivi, and H. Vömel, 2014: Reference quality upper-air measurements: Gruan data processing for the vaisala rs92 radiosonde. *Atmospheric Measurement Techniques*, **7 (12)**, 4463–4490, https://doi.org/10.5194/amt-7-4463-2014.

Durre, I., R. S. Vose, and D. B. Wuertz, 2006: Overview of the integrated global radiosonde archive. *Journal of Climate*, **19 (1)**, 53 – 68, https://doi.org/10.1175/JCLI3594.1.

Frehlich, R. G., and R. D. Sharman, 2010: Equivalence of velocity statistics at constant pressure or constant altitude. *Geophysical Research Letters*, **37 (8)**, https://doi.org/https://doi.org/10.1029/2010GL042912.

Gage, K. S., and G. D. Nastrom, 1986: Theoretical interpretation of atmospheric wavenumber spectra of wind and temperature observed by commercial aircraft during gasp. *Journal of Atmospheric Sciences*, **43 (7)**, 729 – 740, https://doi.org/10.1175/1520-0469(1986)043<0729:TIOAWS>2.0.CO;2.

Gao, X., and J. W. Meriwether, 1998: Mesoscale spectral analysis of in situ horizontal and vertical wind measurements at 6 km. *Journal of Geophysical Research: Atmospheres*, **103 (D6)**, 6397–6404, https://doi.org/https://doi.org/10.1029/97JD03074.

Graw Radiosondes GmbH & Co. KG, 2024: *Radiosonde DFM-17: High accuracy GNSS radiosonde with PTU measurements*. Nürnberg, Germany, Graw Radiosondes GmbH & Co. KG, URL https://www.graw.de/fileadmin/cms_upload/en/Resources/pdf/DB-DFM-17-DE_V02.00.pdf, document version V02.00.

Julian, P. R., W. M. Washington, L. Hembree, and C. Ridley, 1970: On the spectral distribution of large-scale atmospheric kinetic energy. *Journal of Atmospheric Sciences*, **27 (3)**, 376 – 387, https://doi.org/10.1175/1520-0469(1970)027<0376:OTSDOL>2.0.CO;2.

Khairoutdinov, M. F., and D. A. Randall, 2003: Cloud resolving modeling of the arm summer 1997 iop: Model formulation, results, uncertainties, and sensitivities. *Journal of the Atmospheric Sciences*, **60 (4)**, 607–625.

Kolmogorov, A. N., 1941: The local structure of turbulence in incompressible viscous fluid for very large reynolds. *Numbers. In Dokl. Akad. Nauk SSSR*, **30**, 301.

Kraichnan, R. H., 1967: Inertial ranges in two-dimensional turbulence. *Physics of fluids*, **10 (7)**, 1417.

Lindborg, E., 1999: Can the atmospheric kinetic energy spectrum be explained by two-dimensional turbulence? *Journal of Fluid Mechanics*, **388**, 259–288, https://doi.org/10.1017/S0022112099004851.

Lindborg, E., 2006: The energy cascade in a strongly stratified fluid. *Journal of Fluid Mechanics*, **550**, 207–242, https://doi.org/10.1017/S0022112005008128.

Lindborg, E., K. K. Tung, G. D. Nastrom, J. Y. N. Cho, and K. S. Gage, 2010: Comment on "reinterpreting aircraft measurement in anisotropic scaling turbulence" by lovejoy et al. (2009). *Atmospheric Chemistry and Physics*, **10 (3)**, 1401–1402, https://doi.org/10.5194/acp-10-1401-2010.

Lovejoy, S., and D. Schertzer, 1985: Generalized scale invariance in the atmosphere and fractal models of rain. *Water Resources Research*, **21 (8)**, 1233–1250, https://doi.org/https://doi.org/10.1029/WR021i008p01233.

Lovejoy, S., and D. Schertzer, 2010: Towards a new synthesis for atmospheric dynamics: Space–time cascades. *Atmospheric Research*, **96 (1)**, 1–52, https://doi.org/https://doi.org/10.1016/j.atmosres.2010.01.004.

Lovejoy, S., and D. Schertzer, 2011: Space-time cascades and the scaling of ecmwf reanalyses: Fluxes and fields. *Journal of Geophysical Research: Atmospheres*, **116 (D14)**, https://doi.org/https://doi.org/10.1029/2011JD015654.

Lovejoy, S., and D. Schertzer, 2013: *The weather and climate: emergent laws and multifractal cascades*. Cambridge University Press.

Lovejoy, S., A. F. Tuck, S. J. Hovde, and D. Schertzer, 2007: Is isotropic turbulence relevant in the atmosphere? *Geophysical Research Letters*, **34 (15)**, https://doi.org/https://doi.org/10.1029/2007GL029359.

Lovejoy, S., A. F. Tuck, D. Schertzer, and S. J. Hovde, 2009: Reinterpreting aircraft measurements in anisotropic scaling turbulence. *Atmospheric Chemistry and Physics*, **9 (14)**, 5007–5025, https://doi.org/10.5194/acp-9-5007-2009.

Nastrom, G., K. S. Gage, and W. Jasperson, 1984: Kinetic energy spectrum of large-and mesoscale atmospheric processes. *Nature*, **310 (5972)**, 36–38.

Nastrom, G. D., and K. S. Gage, 1983: A first look at wavenumber spectra from gasp data. *Tellus A*, **35A (5)**, 383–388, https://doi.org/https://doi.org/10.1111/j.1600-0870.1983.tb00213.x.

Nastrom, G. D., and K. S. Gage, 1985: A climatology of atmospheric wavenumber spectra of wind and temperature observed by commercial aircraft. *Journal of Atmospheric Sciences*, **42 (9)**, 950 – 960, https://doi.org/10.1175/1520-0469(1985)042<0950:ACOAWS>2.0.CO;2.

Obukhov, A., 1959: Effect of archimedean forces on the structure of the temperature field in a turbulent flow. *Dokl. Akad. Nauk SSSR*, Vol. 125, 1246–1248.

Pinel, J., S. Lovejoy, D. Schertzer, and A. F. Tuck, 2012: Joint horizontal-vertical anisotropic scaling, isobaric and isoheight wind statistics from aircraft data. *Geophysical Research Letters*, **39 (11)**, https://doi.org/https://doi.org/10.1029/2012GL051689, https://agupubs.onlinelibrary.wiley.com/doi/pdf/10.1029/2012GL051689.

Schertzer, D., and S. Lovejoy, 1985: The dimension and intermittency of atmospheric dynamics. *Turbulent Shear Flows 4*, L. J. S. Bradbury, F. Durst, B. E. Launder, F. W. Schmidt, and J. H. Whitelaw, Eds., Springer Berlin Heidelberg, Berlin, Heidelberg, 7–33.

Schertzer, D., I. Tchiguirinskaia, S. Lovejoy, and A. F. Tuck, 2012: Quasi-geostrophic turbulence and generalized scale invariance, a theoretical reply. *Atmospheric Chemistry and Physics*, **12 (1)**, 327–336, https://doi.org/10.5194/acp-12-327-2012.

Tennekes, H., and J. L. Lumley, 1972: *A First Course in Turbulence*. The MIT Press, https://doi.org/10.7551/mitpress/3014.001.0001.

Vaisala Oyj, 2017: Vaisala radiosonde rs41 measurement performance. White Paper B211356EN-B, Vaisala Oyj. URL https://www.vaisala.com/sites/default/files/documents/WEA-MET-RS41-Performance-White-paper-B211356EN-B-LOW-v3.pdf, version 3.

VanZandt, T. E., 1982: A universal spectrum of buoyancy waves in the atmosphere. *Geophysical Research Letters*, **9 (5)**, 575–578, https://doi.org/https://doi.org/10.1029/GL009i005p00575, https://agupubs.onlinelibrary.wiley.com/doi/pdf/10.1029/GL009i005p00575.

Vömel, H., A. Sorooshian, C. Robinson, T. J. Shingler, K. L. Thornhill, and L. D. Ziemba, 2023: Dropsonde observations during the aerosol cloud meteorology interactions over the western atlantic experiment. *Scientific Data*, **10 (1)**, 753, https://doi.org/10.1038/s41597-023-02647-5.

Wang, J. J., and Coauthors, 2015: A long-term, high-quality, high-vertical-resolution gps dropsonde dataset for hurricane and other studies. *Bulletin of the American Meteorological Society*, **96 (6)**, 961 – 973, https://doi.org/10.1175/BAMS-D-13-00203.1.

Wiin-Nielsen, A., 1967: On the annual variation and spectral distribution of atmospheric energy. *Tellus*, **19 (4)**, 540–559, https://doi.org/https://doi.org/10.1111/j.2153-3490.1967.tb01507.x.